

Dynamic behaviors of viscous damper on concrete archaized building with lintel-column joint

Jiayang Xue^{*1}, Jinshuang Dong^{1a} and Yan Sui^{1,2b}

¹School of Civil Engineering, Xi'an University of Architecture and Technology, Xi'an, Shaanxi, China

²State Key Laboratory of Architecture Science and Technology in West China, Xi'an, Shaanxi, China

(Received July 9, 2016, Revised December 18, 2017, Accepted January 4, 2017)

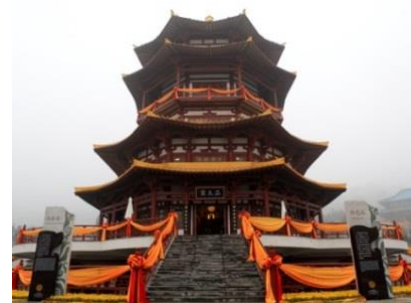
Abstract. In order to analyze the vibration control effect of viscous damper in the concrete archaized buildings with lintel-column joints under seismic action, 3 specimens were tested under dynamic excitation. Two specimens with viscous damper were defined as the controlled component and one specimen without viscous damper was specified as the non-controlled component. The loading process and failure patterns were obtained from the test results. The failure characteristics, skeleton curves and mechanical behavior such as the load-displacement hysteretic loops, load carrying capacity, degradation of strength and rigidity, ductility and energy dissipation of the joints were analyzed. The results indicate that the load-bearing capacity of the controlled component is significantly higher than that of the non-controlled component. The former component has an average increase of 27.4% in yield load and 22.4% in ultimate load, respectively. Meanwhile, the performance of displacement ductility and the ability of energy dissipation for the controlled component are superior to those of the non-controlled component as well. Compared with non-controlled component, equivalent viscous damping coefficients are improved by 27.3%-30.8%, the average increase is 29.0% at ultimate load for controlled component. All these results reflect that the seismic performance of the controlled component is significantly better than that of the non-controlled component. These researches are helpful for practical application of viscous damper in the concrete archaizing buildings with lintel-column joints.

Keywords: archaized buildings; dynamic test; seismic behavior; viscous damper

1. Introduction

National feature, local culture and architectural context are among the important elements to be considered for increasing building ornamental requirements. The traditional construction of archaized buildings is one of the rare treasures and beautiful representation of the Chinese architectural culture (Xie 2006, Tian 2012). Therefore, it is important to study and represent characteristics of the archaized buildings (also called traditional style buildings) in design of modern architecture, as shown in Fig. 1.

Presently, most of the research on mechanical properties of archaized buildings is just in the beginning phase and an integrated technical system has not been formed. And researches about archaized buildings mainly focus on the steel archaized buildings (Xue *et al.* 2015, 2016). In order to investigate the seismic behavior of RC column-beam joint built in traditional style, 4 specimens with a scale of 1:1.5 were tested under low-cyclic reversed loading at Xi'an University of Architecture and Technology. Compared with normal RC column-beam joint, the displacement



(a) Female Springs



(b) Shaanxi History Museum

Fig. 1 Archaized buildings

*Corresponding author, Ph.D.

E-mail: jiayang_xue@163.com

^aLecturer

E-mail: mlcxll@163.com

^bAssociate Professor

E-mail: suiyanmy@163.com

ductility factor and the energy dissipation coefficient during limit stage of RC column-double beam joint built in traditional style are smaller, and the ductility and energy dissipation are worse. Xue (2015, 2016) have studied the failure mode, hysteretic performance, and ductility of traditional style building.

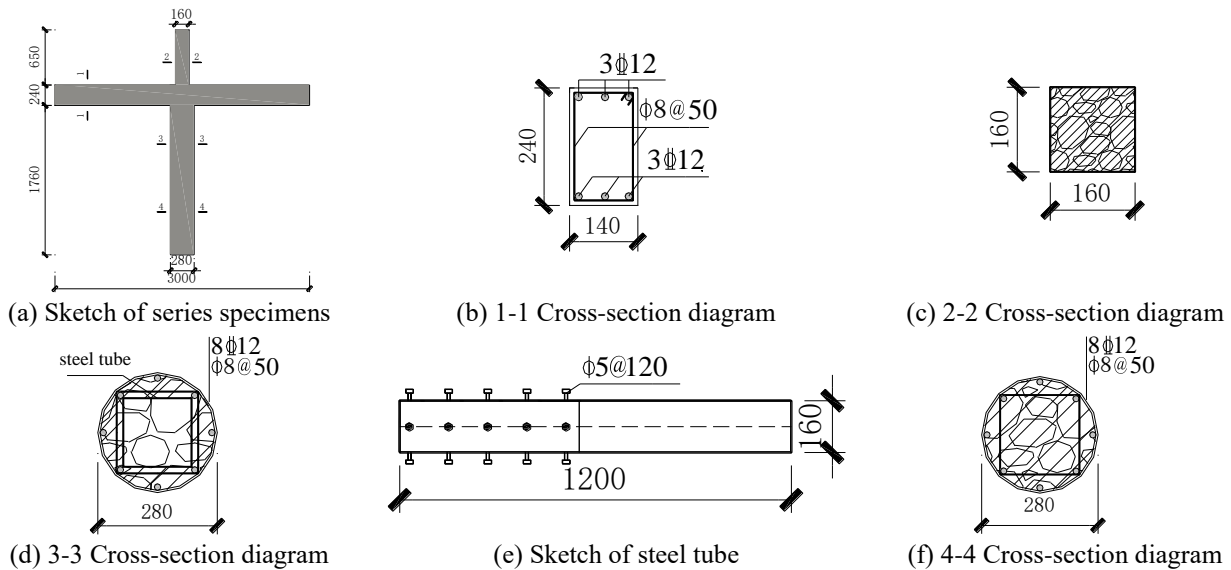


Fig. 2 Details of joints

How to identify and improve the mechanical properties of archaized buildings has become an urgent key technological issue (Xie *et al.* 2015, Li 2014 and Wang *et al.* 2011). At the present time, energy-dissipating structure has been proved to be a type of seismic structure with good performance based on the theoretical researches and engineering practice among many countries. In theory, the definition of energy dissipation means some parts of the structure are designed as energy-dissipating components, or viscous dampers are located at certain locations (such as beam-column joints, junction points and so on). The structure and energy dissipation dampers are mainly in elastic state under wind load or frequent earthquake load to make sure that the structure can operate and function properly with enough lateral stiffness. The inelastic strains start to appear on the energy dissipation parts and the energy dissipation dampers under medium earthquake and rare earthquake conditions. Energy dissipation components or the dampers can absorb most of energy from the seismic waves, thus, to protect the main structure from severe seismic excitations (Abdi *et al.* 2015, Parmar *et al.* 2014, Zhu *et al.* 2014). The Beijing Exhibition Center, built in 1953, did not meet the seismic fortification intensity 8 of Beijing region. Based on the existing conditions, 116 viscous dampers have been used to provide a comprehensive seismic strengthening design for the building. After that reinforcement, the analyses results indicate that the structure is elastic under frequent earthquake and intermediate earthquake conditions and the main structure has good performance under rare earthquake conditions. The inter-story displacement ratio of structure is well within 1/350. Therefore, the seismic strengthening design for the building has achieved the desired purposes (Song 2001). The Kagoshima Airport terminal building is a 3-story R.C. framed structure constructed in 1972. The original story shear capacity was far less than the demand of the level II earthquake loading of current seismic code in Japan. 28 velocity-dependent damper walls were added to the building frame location. As a result, the damper walls increased the effective stiffness of the structure during seismic excitation and reduced the effective period and the

spectral displacement. Almost all of the existing structural elements remained in elastic capacity and minimal retrofit of existing frames or foundation work was required (Zheng *et al.* 2006).

Currently, there is no research on the concrete archaized buildings with lintel-column joints with viscous damper. The experimental research on seismic performance of this type of structure will not only help us to understand the theory and method of archaizing buildings design, but also can provide reference to the engineering practice of the similar structure. Therefore, the study on this field is an important subject with great theoretical significance and practical engineering value.

In this study, 3 specimens were tested under dynamic loading. Two specimens with viscous damper were specified as the controlled component. One specimen without viscous damper was defined as the non-controlled component. Dynamic loading laws were adopted, and the failure process and patterns were obtained. The failure characteristics, skeleton curves, mechanical behavior such as the load-displacement hysteretic loops, load carrying capacity, degradation of strength and rigidity, ductility and energy dissipation of the joints were analyzed.

2. Outline of specimens

2.1 Design of specimens

A total of 3 concrete archaizing buildings with lintel-column joints with viscous damper were constructed and tested, the specimen number is SLJ-1, SLJ-2 and SLJ-3, respectively. The SLJ-1 was the non-controlled component without viscous damper. As shown in Fig. 2. The specimens were selected with reasonable dimensions reinforced with sufficient longitudinal bars and hoops, to avoid the shear failure occurring before flexural failure, the concrete crush occurring before reinforcements yielded, and the anchorage and cohesion failure of reinforcements occurring before member damaged.

Table 1 Mechanic performance index of steel bars and tube

Steel tube/Steel bars(mm)	f_y /MPa	$\varepsilon_y/10^{-3}$	f_u /MPa	E_s /MPa	$\delta/\%$
$t=5.5$	336.5	1674	463.3	2.01	32.9
$\phi 8$	323.5	1570	400.0	2.06	35.6
$\Phi 12$	450.1	2296	586.7	1.96	30.8

Note: f_y -Yield strength; ε_y -Yield strain; f_u -Ultimate load; E_s -Elasticity modulus; δ -Elongation

Table 2 Design parameter of viscous damper

No.	F /kN	C /(kN*s/m)	α	Design displacement/mm
SLJ-2	80	88	0.36	± 30
SLJ-3	50	60	0.30	± 30



Fig. 3 Sketch of viscous damper

Axial-force-ratio refers to the ratio of the combined axial compressive force (including seismic effects) to the design value of column which is the product of the column cross sectional area and the specified concrete compressive strength. Therefore, Axial-force-ratio can be determined by the Eq. (1)

$$n = N / (f_c A_c + f_{ss} A_{ss}) \quad (1)$$

Where: n -axial-force-ratio; N -combined axial compressive force; f_c -design value of axial compressive strength of concrete; A_c -the cross-section area of concrete without steel tube; f_{ss} -design value of axial compressive strength of steel tube; A_{ss} -the cross-section area of steel tube. $n=0.25$ and $N=367$ kN.

Concrete with grade C40 was adopted in all beams and columns. Mechanic performance index was shown in Table 1. The cube compressive strength of concrete is 51.4 MPa.

2.2 Choice of viscous damper

Viscous dampers provide a force which is proportional to the relative velocity between the ends of the damper, to help structures resist earthquake motion. The damping law is defined as Eq. (2)

$$F = CV^\alpha \quad (2)$$

Where: F is the damper force; C is the damper coefficient; V is relative velocity; α is damper exponent. For linear viscous damper, $\alpha=1$, while for nonlinear viscous damper, $\alpha \neq 1$.

No spring force is considered in this equation for the reason that damper force varies with different absolute

velocity. For a given velocity the force will be the same at any point in the stroke. All the external lateral loads should be resisted by structure itself since that dampers would not provide additional restoring force although the damper force should be 0.30-0.75 power of its relatively velocity for most viscous dampers (Housner 1997). The design parameters of viscous damper as shown in Table 2.

The type of viscous damper and its parameters can be determined under the following method. Firstly, the length and force of viscous damper should be determined under the Caifen modular system of ancient Chinese building citations, and on this basis, the range of the main parameter (i.e. damping coefficient and damping exponent) can be determined under the type of viscous damper provided by manufacturer, the size of viscous damper is 770 mm. Finally, the optimized result of these parameters can be obtained by means of optimization study. As shown in Fig. 3.

2.3 Experimental setup and procedure

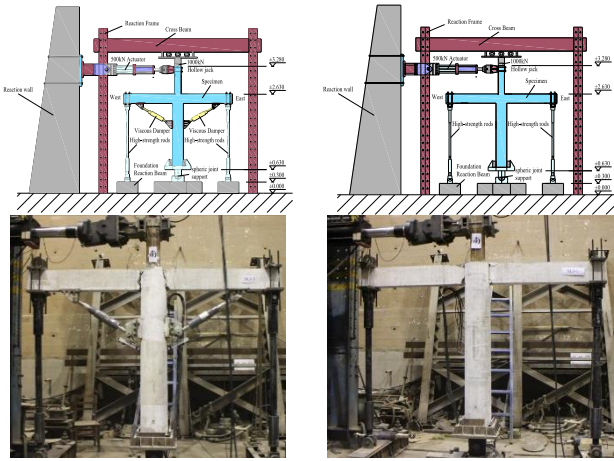
The joints were placed at their characteristic position in a typical RC frame and were mounted on a stiff steel frame as shown schematically in Fig. 4. In this configuration, the column longitudinal axis was vertical, and the beam longitudinal axis was horizontal. Testing of each model began by slowly applying loads to simulate axial loading of the column. This was accomplished by a 1000-kN hydraulic loading jack. During the testing, application of the axial load was controlled manually and kept constant at a level of 360-kN for all specimens. The experiment was conducted in Structural Engineering Key Laboratory at Xi'an University of Architecture and Technology.

Once the full axial load had been applied, dynamic cyclic-lateral loads were simulated by applying an alternating force to the end of the column-end through an idealized pin. This force was applied in a dynamic-cyclic pattern using a horizontally positioned 500-kN MTS actuator (± 250 mm). Data from the load cell and the actuator's displacement transducer was recorded by using a computer controlled data acquisition system.

The termination of test is at the condition that the horizontal bearing capacity of test specimen reduced to 85% and below of the ultimate load, or the inter-story displacement exceeded the ultimate displacement.

Generally, quasi-static test was commonly adopted in the traditional seismic resistant testing of the joints. To some extent quasi static loading method can reflect the mechanical characteristics and seismic performance of the specimens. But in essence, quasi-static test is static test without the time histories, which couldn't completely reflect the actual influence of earthquake effects on structures.

Therefore, considering that the speed-nonlinear-relevant type viscous damper was adopted in the test, the loading method shall be determined by controlling displacement (amplitude) and loading frequency. The loading form was sine wave pattern. The controlling displacement (amplitude) and loading frequency were determined by Code requirements specified in Seismic Design of Building (GB50011-2010) (National Standard of PRC 2010) (also called the Seismic Code) and The Chinese seismic intensity



(a) Loading device of controlled joints (b) Loading device of uncontrolled joints

Fig. 4 Loading device

Table 3 The test loading mode

Condition	$a^*/(\text{cm/s}^2)$	s/mm	f/Hz	condition	$a^*/(\text{cm/s}^2)$	s/mm	f/Hz
1	50	5	1.59	7	500	53	1.55
2	100	8	1.78	8	570	65	1.50
3	150	11	1.86	9	585	77	1.39
4	250	15	2.05	10	600	88	1.31
5	350	27	1.81	11	700	106	1.29
6	460	40	1.71	12	800	133	1.23

Note: a -acceleration; s -controlling displacement; f -loading frequency

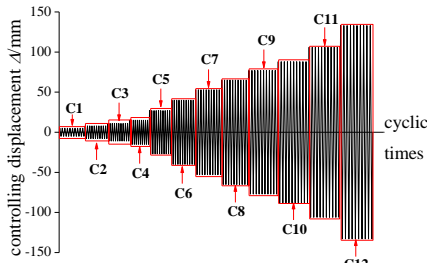


Fig. 5 Sketch of loading condition

scale (GB/T 17742-2008). The experimental procedure was determined by guidelines for the testing of seismic isolation and energy dissipation devices adopted by Dampers for vibration energy dissipation of buildings (JGT209-2012) (National Standard of PRC 2012).

The displacement-controlled loading sequence for each specimen consisted of ten cycles at a series of progressively increasing displacement amplitudes in each hoop. The loading history is illustrated in Table 3. The plot of applied cyclic displacement is shown in Fig. 5 below.

2.4 Measuring scheme

Fig. 6 represents the arrangement of strain gauges, the measuring scheme includes: 1) steel strain and crack propagation of joint area; 2) crack propagation and

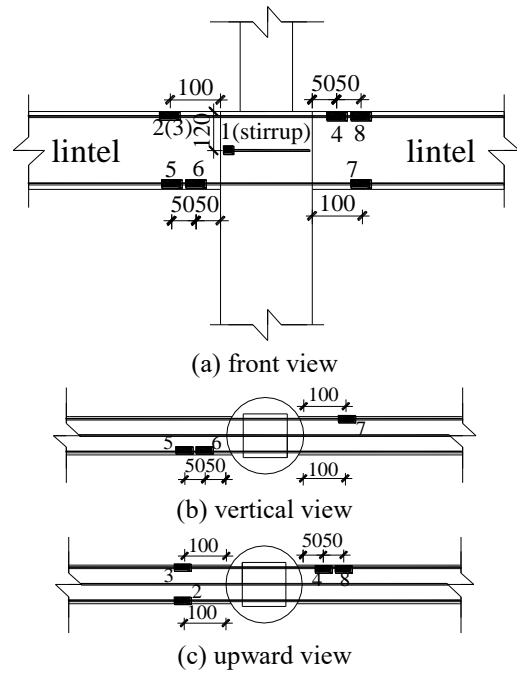


Fig. 6 Arrangement of strain gauges

deformation of plastic-hinge region of beam-end; 3) steel strain and bearing capacity of beam-end.

All of the electric resistance strain gauges were coated by epoxy resin to ensure the normal working condition of gauges. The strain data was collected by an 8-channel dynamic strain gauge data-acquisition device (model: DC-104R Japan) in real time, and load-displacement of column-end was recorded using a computer controlled data acquisition system. The arrangement of strain gauges was illustrated in Fig. 6.

3. Failure modes and force mechanism research

3.1 Failure modes

All specimens have roughly the same process of failure. The whole process can be divided into 4 stages.

- Cracking stage: Once the full axial load had been applied, dynamic cyclic-lateral loads were simulated by applying an alternating force to the end of the column-end through an idealized pin. Before the control displacement is 8mm (condition 2), there is a linear relation between horizontal load and displacement, and the specimen is still in elastic state, there are no clear signs of destruction. Only some small and irregular diagonal cracks appeared in the south and north surface of beam as the horizontal displacement increased. The crack load of SLJ-1, SLJ-2 and SLJ-3 is 14.6 kN, 15.8 kN and 16.8 kN, respectively. Compared with SLJ-1, the crack load is increased by 8.3% and 15.3% respectively. The crack loads for all specimens with little difference, which indicated that the damper is not effective and could not provide significant effects to improve the crack-control performance in the cracking stage. Since the amplitude of applied displacement is low, therefore, the velocity is low and viscous damper is not able

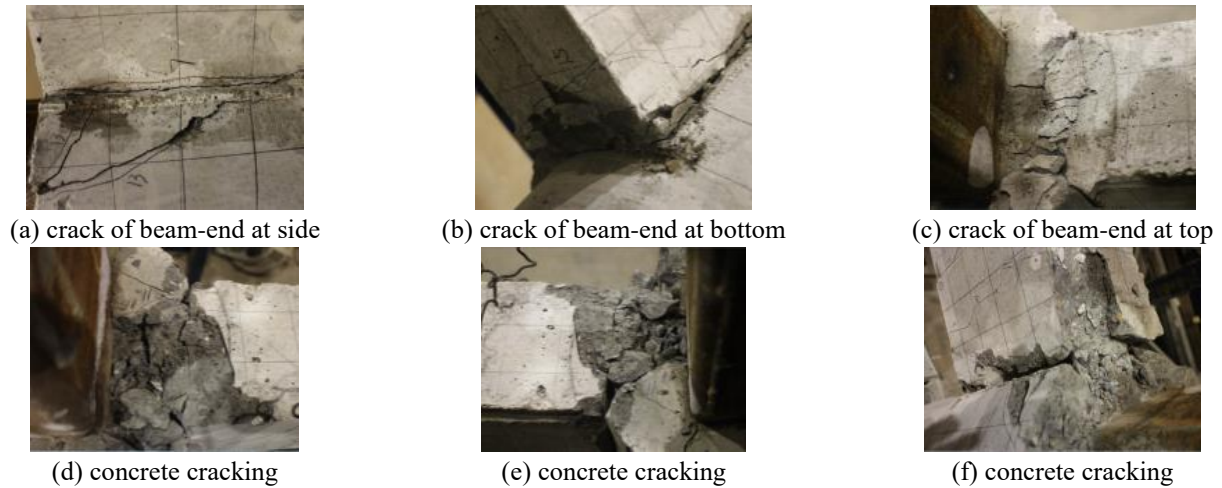


Fig. 7 Failure modes of SLJ-1

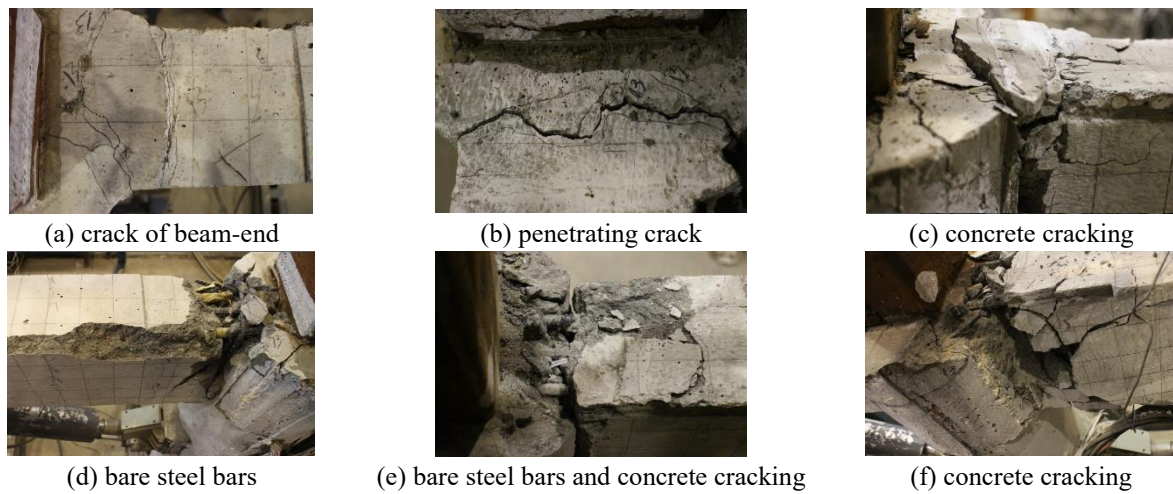


Fig. 8 Failure modes of specimens with viscous

to function and produce resistant force. For this reason viscous damper effect is negligible in the cracking stage.

- Yield stage: As the horizontal displacement increased at the column-end, diagonal cracks started to develop and extend slowly. The cracks in the joint core zone were distributed roughly symmetrically, accompanying with some new cracks. Some X-shape cracks were also formed. Based on the data collected from the devices, beam-end has reached the elastic-plastic phase, but the joint core zone was still in the elastic stage. When the control displacement is 27 mm (condition 5), the measured strain values is exceed the yield strain values as shown in table 1 of paper and the load-displacement hysteresis curve with an obvious inflection points, in this case, elastoplastic phase of specimens could be identified. The average maximum damping force of SLJ-2 and SLJ-3 are 20.5 kN and 18.7 kN, respectively; the average maximum displacement of viscous damper is 6.8 mm and 7.9 mm for SLJ-2 and SLJ-3, respectively.

- Ultimate stage: As the horizontal displacement increased at the column-end, the specimens reached their peak load. During the process, diagonal cracks widened and extended quickly. Some surface concrete of the specimens started to crush and fall off. At the beam-end of specimens,

concrete spalled off and some diagonal cracks extended to both column bottoms. When the control displacement is 40 mm (condition 6), degradation on the horizontal load and displacement hysteresis curve of SLJ-1 was found and the peak load was 33.9 kN. When the control displacement is 65 mm (condition 8) and 53 mm (condition 7), degradation on the horizontal load and displacement hysteresis curve of SLJ-2 and SLJ-3 were found and the peak load was 47.8 kN and 45.2 kN, respectively.

- Failure stage: When the horizontal loading exceeded the peak loading, the bearing capacity began to decline. As the horizontal displacement increased at the column-end, the falling and crushing of the concrete became more significant, and some steel bars started to expose. Some loud sounds of concrete crushing were heard. For the joint without viscous damper, the falling and crushing of concrete were more serious. The concrete at the beam-end fell off seriously and steel bars became exposed. Hinge points were formed at beam-end and the specimen became geometrically unstable. At this time, the horizontal load was decreased to less than 85 percent of the peak load and the vertical load cannot be sustained, therefore the experimental process was stopped as shown in Fig. 7.

For the joint with viscous damper, bearing capacity is better than the joint without viscous damper. As the

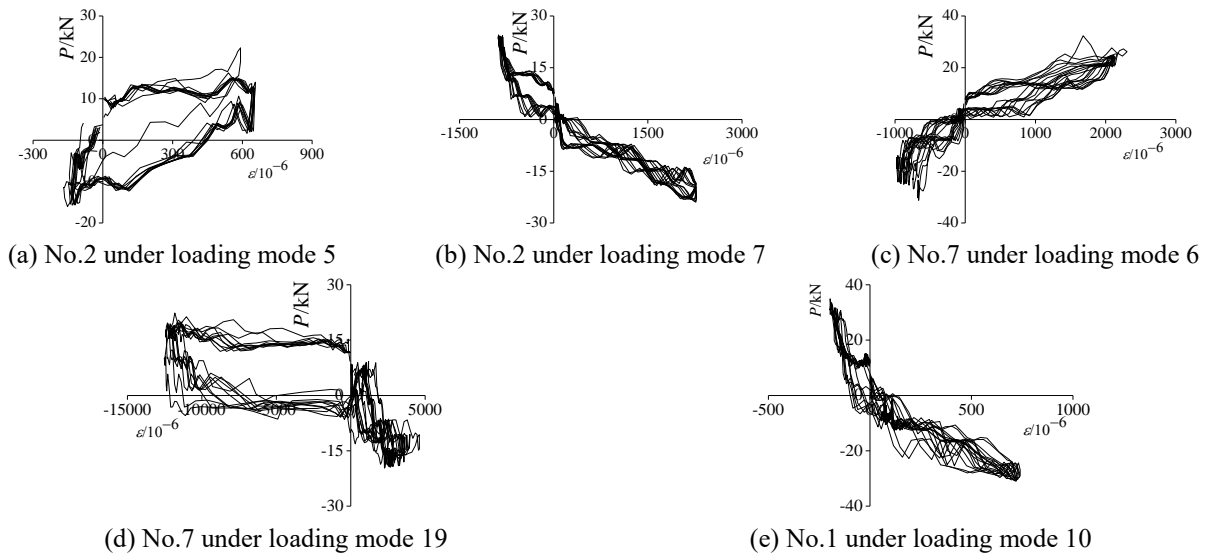


Fig. 9 Cyclic load-strain curves of SLJ-1

horizontal displacement increased at the column-end, the falling and crushing of the concrete were gradually increasing and the cracks developed slowing at beam-end. The specimen maintained as the geometrically stable system due to the viscous damper as a brace. When the control displacement is 133 mm (condition 12), the average maximum damping force of SLJ-2 and SLJ-3 are 32.6 kN and 34.2 kN, respectively; the average maximum displacement of viscous damper is 24.6 mm and 25.7 mm for SLJ-2 and SLJ-3, respectively. Eventually, for SLJ-2, test was not terminated until the ultimate load declined to 77% of peak load positively and 78% of peak load negatively, for SLJ-3, the values is 82% and 80%, respectively, the horizontal load was decreased to less than 85 percent of the peak load, the experiment was terminated, as shown in Fig. 8.

3.2 Force mechanism research

The whole failure process for the concrete archaized buildings with lintel-column joint can be described as following:

At the initial loading stage, when the horizontal rotation angle was less 1/200, there were no visible cracks and residual deformation, the horizontal loading and displacement are in linear relation, the area of hysteretic curves is small, and the recoverable elastic strain energy is a major part of energy consumption of the specimens. As the horizontal displacement started to increase at the column-end, the falling and crushing of concrete became more significant, some steel bars started to expose, and cracks appeared to run through the zone of beam-end. For the joint without viscous damper, the plastic hinges appeared at the beam-end and the specimen had become geometrically unstable. Eventually the horizontal load was decreased to less than 85 percent of the peak load and the vertical load cannot be sustained, which caused the experiment to stop. For the joints with viscous damper, the specimen was kept as a geometrically stable system due to the viscous damper as a bracing system. The decreasing stage of the horizontal

loading and displacement were smoother. The experimental process was stopped when the horizontal load was decreased to less than 85 percent of the peak load.

4. Experimental results

4.1 Strain analysis

Taking specimen SLJ-1 and SLJ-2 as examples, the strains of the beam end and core area were analyzed to investigate the strain -stress mechanism of the concrete archaized buildings with lintel-column joint. Strain gage No. 2, No. 7 and No. 1, which were placed in the hinged area and core area of the joints, respectively, were selected to be analyzed. Curve of loading vs. strain for each measure point were shown in Figs. 7 and 8.

4.1.1 Specimen SLJ-1

Gage No. 2 was placed on the top of beam end to record the strain of longitudinal reinforcement. The load vs. strain curve of this gage was shown in Fig. 9(a) and 9(b). When the control displacement was 27 mm, the maximum strain value was within $630 \mu\epsilon$, which was smaller than the yield value. Almost no residual strain existed when unloaded, which indicated that specimen was in the elastic stage. When the control displacement was 53 mm, the strain value achieved $2300 \mu\epsilon$, which obviously exceeded the yield value. The residual strain appeared when unloaded and the specimen was in the elasto-plastic stage.

Gage No. 7 was placed on the bottom of beam end to record the strain of longitudinal reinforcement. The load vs. strain curve for this gage was shown in Fig. 9(c) and 9(d). When the control displacement was 40 mm, the maximum strain value was within $2400 \mu\epsilon$, which obviously exceeded the yield value. The specimen was in elasto-plastic stage. When the control displacement was 77 mm, the strain value achieved $11600 \mu\epsilon$ with larger residual strain.

Gage No. 1 was placed on the core area of the joint. The

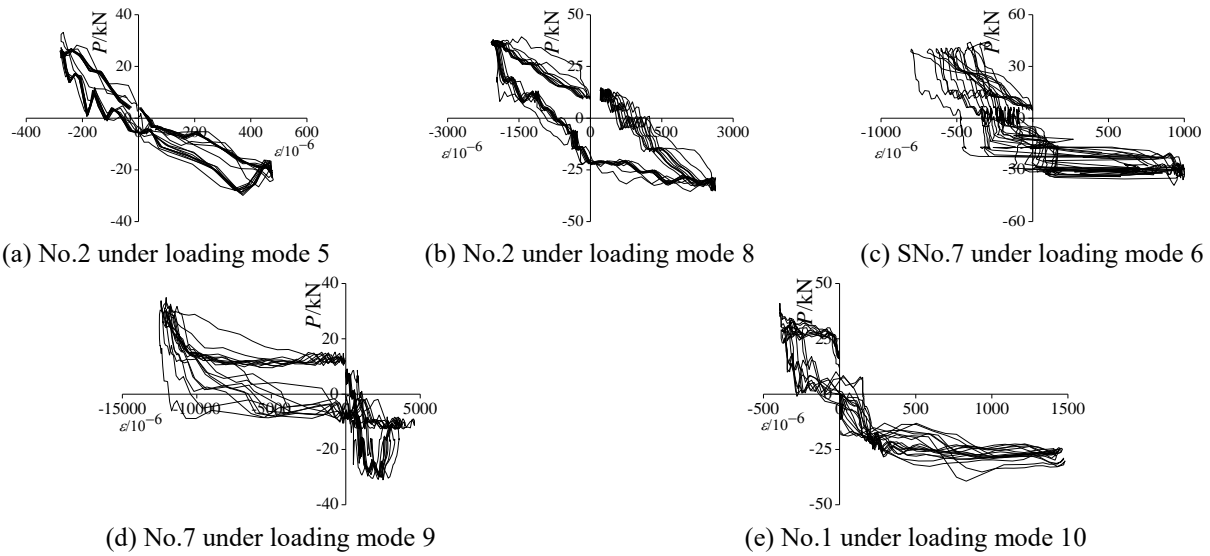


Fig. 10 Cyclic load-strain curves of SLJ-2

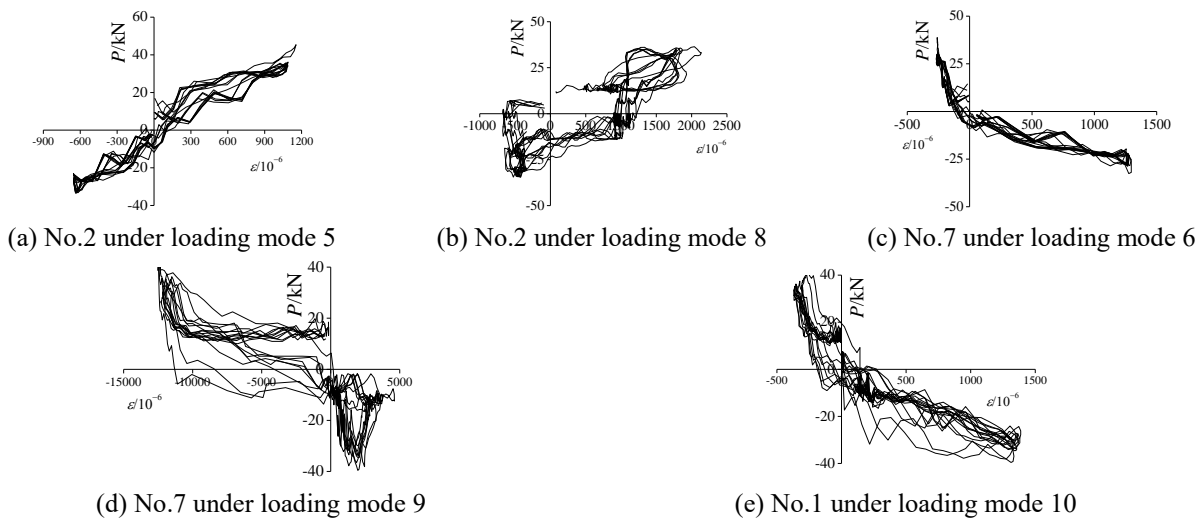


Fig. 11 Cyclic load-strain curves of SLJ-3

load vs. strain curve was shown in Fig. 9(e). When the control displacement was 88 mm, the maximum strain value of stirrup was about $860 \mu\epsilon$, which was smaller than the yield value. Almost no residual strain existed when unloaded, which indicated that specimen was in the elastic stage. This condition met the goal of “strong column-weak beam, strong shear capacity-weak bending capacity, strong joint-weak component” requirement in seismic design. Since the hinged area happened in the beam end, combined with the failure mode we observed in the test, we could determine the failure mechanism as beam-hinged mechanism.

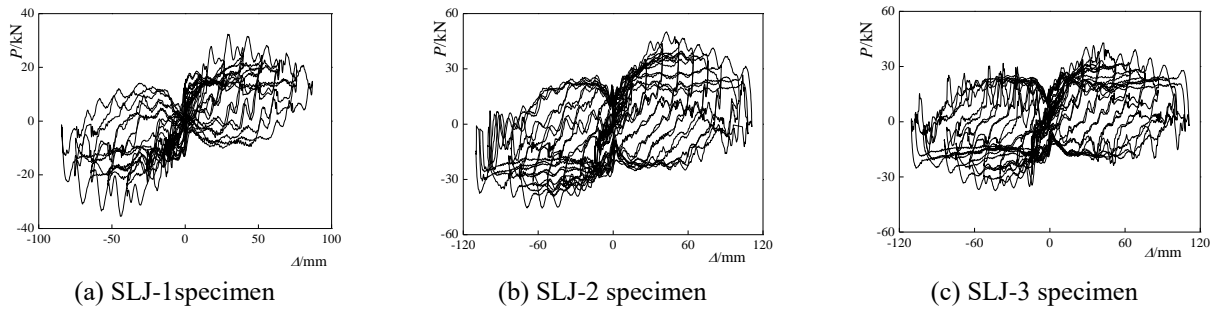
4.1.2 Specimen SLJ-2

Gage No. 2 was placed on the top of beam end to record the strain of longitudinal reinforcement. The load vs. strain curve was shown in Fig. 10(a) and 10(b). When the control displacement was 27 mm, the maximum strain value was within $480 \mu\epsilon$, which was smaller than the yield value and the corresponding strain value of specimen SLJ-1. Almost no residual strain existed when unloaded, which indicated

that specimen was in the elastic stage. When the control displacement was 77 mm, the strain value achieved $2600 \mu\epsilon$, which obviously exceeded the yield value. Since the residual strain existed when unloaded, the specimen was in elasto-plastic stage.

Gage No. 7 was placed on the bottom of the beam end to record the strain of longitudinal reinforcement. The load vs. strain curve was shown in Fig. 10(c) and 10(d). When the control displacement was 40 mm, the maximum strain value was within $980 \mu\epsilon$, which indicated that the specimen was in elasto-plastic stage. When the control displacement was 77 mm, the strain value achieved $11000 \mu\epsilon$ with larger residual strain, which indicated that the damper could reduce the strain response of specimen before yielding but provide no influence after yielding.

Gage No. 1 was placed on the core area of the joint. The load vs. strain curve was shown in Fig. 10(e). When the control displacement was 88 mm, the maximum strain value of stirrup was about $1500 \mu\epsilon$, which was a little larger than the yield value. Almost no residual strain existed when unloaded, which indicated that specimen started to enter

Fig. 12 Hysteretic loops of $P-\Delta$

into the elastic stage and met the goal of “strong column-weak beam, strong shear capacity-weak bending capacity and strong joint-weak component” requirement in seismic design. The hinged area happened in the beam end. Combined with the failure modes observed in the test, we could determine that the failure mechanism was the beam-hinged mechanism.

4.1.3 Specimen SLJ-3

Gage No. 2 was placed on the top of beam end to record the strain of longitudinal reinforcement. The load vs. strain curve was shown in Fig. 11(a) and 11(b). When the control displacement was 27 mm, the maximum strain value was within $1100 \mu\epsilon$. Almost no residual strain existed when unloaded, which indicated that specimen was in the elastic stage. When the control displacement was 65 mm, the strain value achieved $2200 \mu\epsilon$, which is equal to the yield value. Which means the specimen was in elastoplastic stage.

Gage No. 7 was placed on the bottom of the beam end to record the strain of longitudinal reinforcement. The load vs. strain curve was shown in Fig. 11(c) and 11(d). When the control displacement was 77 mm, the strain value achieved $12000 \mu\epsilon$ with larger residual strain, which indicated that the damper could reduce the strain response of specimen before yielding but provide no influence after yielding.

Gage No. 1 was placed on the core area of the joint. The load vs. strain curve was shown in Fig. 11(e). When the control displacement was 88 mm, the maximum strain value of stirrup was about $1400 \mu\epsilon$. Almost no residual strain existed when unloaded, which indicated that specimen met the goal of “strong column-weak beam, strong shear capacity-weak bending capacity and strong joint-weak component” requirement in seismic design. The hinged area happened in the beam end.

4.2 Load vs. displacement hysteresis curve

Hysteresis curve is mainly composed of hysteresis loops, which reflect the seismic performance, bearing capacity, ductility, stiffness degradation, and energy-dissipation ability of structure comprehensively. It can be viewed as an important basis for elastoplastic analysis. The hysteresis curves for 3 specimen obtained from this experiment were shown in Fig.12, where P was the horizontal load and Δ indicated the corresponding horizontal displacement.

From Fig. 12, the main features of hysteresis curve for

the concrete archaized buildings with lintel-column joint can be listed as follows:

- In general, the force vs. displacement hysteresis curve of all specimens is plumper and a preferable ductility and dissipative capacity.

- The hysteresis curves of specimen with viscous damper are plumer than specimen without viscous damper, and the peak lateral load keep stable with a large lateral displacement increment of specimen with viscous damper, which indicated that the joints with viscous dampers has better energy-dissipation ability and seismic performance.

- Under low load, the enveloped area of hysteresis curve was tiny and the load and displacement relationship was basically linear, which indicated that the specimen was in the elastic stage with no obvious stiffness degradation and almost no residual deformation when the load returned to zero for all specimens.

- With the displacement increased, the enveloped area became larger, and the hysteresis curve became to incline to the displacement axis with stiffness degradation, which was caused by the yielding of reinforcement at the beam end and the spreading area of concrete crushing. The specimen entered into the elasto-plastic stage from elastic stage. When unloaded, residual deformation was obviously found.

- In the elasto-plastic stage, the curve of load vs. displacement for specimen with viscous dampers had longer hardening stage and its bearing capacity was larger than specimen without viscous damper, which indicated that installation of the viscous damper could improve the load capacity of the specimen.

- For SLJ-2 and SLJ-3, the design parameters of viscous damper are different as shown in table 2. The hysteresis curve of former is plumper than the latter. And the load capacity of SLJ-2 is higher than SLJ-3, which indicates that the design parameters of viscous damper have certain impact on the seismic behavior and load capacity for concrete archaized building with lintel-column joint.

4.3 Load vs. displacement skeleton curve

The yield point can be determined by “Park method” (Elnashai *et al.* 1995). And the yield load P_y and yield displacement Δ_y can be determined at the same time. The damaged load is $0.85P_m$ and its corresponding displacement is Δ_u , where P_m is the ultimate load and its corresponding displacement is Δ_m . Fig. 13 showed the skeleton curve of each specimen, from which each loading point and its value

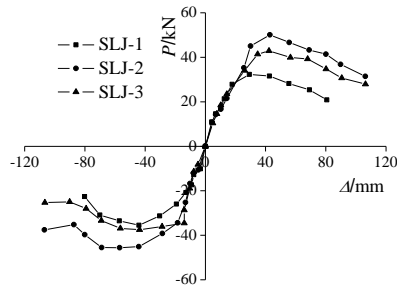


Fig. 13 Skeleton curves of specimens

Table 4 Experimental characteristic values of specimens

Specimen No.	Crack		Yield		Ultimate		Failure	
	P_{cr} /kN	Δ_{cr} /mm	P_y /kN	Δ_y /mm	P_u /kN	Δ_u /mm	P_m /kN	Δ_m /mm
SLJ-1	14.3	7.6	28.3	20.6	32.3	29.2	27.5	58.8
	14.8	7.9	27.5	22.4	35.5	44.7	30.1	70.9
SLJ-2	15.2	7.7	47.2	25.5	50.1	42.9	42.6	73.1
	16.3	7.9	36.8	23.4	45.5	69.7	38.7	81.7
SLJ-3	17.2	7.6	35.8	28.2	42.9	42.3	36.5	81.2
	16.4	7.8	35.1	19.5	37.5	43.7	31.9	71.9

could be obtained, and the values are listed in Table 4.

From Fig. 13 and Table 4, some conclusions can be obtained.

Each specimen went through four stages: cracking, yield, ultimate and damaging, under the constant vertical load and cycle-reversed horizontal load. However, no break points appeared on the skeleton curve, which indicated that the yield phase gradually spread from local to global. According to the test results, the break point occurred when the reinforcement of the beam started yielding.

Based on the comparison with the previous results (Han 2007), it could be concluded that the ductility and energy-dissipation ability of the specimen without viscous damper was worse than those of the reinforced concrete joints. While the specimen with viscous damper was better, where the skeleton curve had longer and tender descending stage. The load capacity of the SLJ-2 and SLJ-3 with viscous dampers was higher than that of the SLJ-1 without viscous damper. Compared with SLJ-1, the crack load of specimens with viscous damper is increased by 8.3% and 15.3% respectively, which indicates that the crack loads for all specimens with little difference. The yield load and ultimate load are increased by 29.6% and 25.3% respectively. When damaged, the descending stage of the skeleton curve for the controlled structure was steeper than that of the uncontrolled component, which demonstrated that installation of dampers could significantly improve the bearing capacity and ductility.

The type of viscous damper for specimen SLJ-2, SLJ-3 are different. From Fig. 13, the specimen SLJ-2 with the viscous damper of higher design load has larger ultimate load capacity. The yield load and ultimate load are increased by 18.5% and 5.8% respectively. The area formed between its skeleton curve and the coordinate axis X was larger, but the descending stage is steeper, which indicated that increasing the design load of viscous damper can

Table 5 Ductility coefficients of specimens

Specimen No.	Δ_y /mm	Δ_m /mm	μ	$\bar{\mu}$
SLJ-1	20.6	58.8	2.85	3.01
	22.4	70.9	3.17	
SLJ-2	25.5	73.1	2.87	3.18
	23.4	81.7	3.49	
SLJ-3	28.2	81.2	2.88	3.28
	19.5	71.9	3.69	

improve the bearing capacity of structure to some extent.

4.4 Ductility and energy-dissipation capacity

The ductility and energy-dissipation indices were listed in Table 5 and Table 6, where ductility coefficient refers to the ratio of the horizontal displacement Δ_m of column when damaged to the horizontal displacement Δ_y of column when yielded.

From the results shown in Table 5 and Table 6 we can conclude that:

- The ductility of the specimen SLJ-1 was lower than that of SLJ-2, SLJ-3, indicating that the viscous damper can improve the ductility of specimens to some extent;
- The ductility of SLJ-2 was lower than that of SLJ-3, demonstrating that different types of viscous damper had different effect on ductility. For the structure in this study, the damper with higher design load can lead to better ductility.
- The equivalent damping coefficient of SLJ-2 and SLJ-3 was higher than that of SLJ-1, obviously. The coefficient was 23.0%-26.9%, 29.2%-31.2% and 43.1%-43.8%, corresponding to the yield load, ultimate load and damage load, respectively, which indicated that the installation of dampers can enhance the energy-dissipation ability of the specimen.
- The design load of damper of SLJ-2 was larger than that of SLJ-3, while the equivalent damping coefficient h_e for the ultimate and damage load was smaller than that of SLJ-3, which indicated that there was no direct relationship between the stiffness degradation and the design load of the viscous damper. It was not the case that damper with higher design load had better energy-dissipation capacity.
- Based on the comparison with the previous results, it can be found that under the ultimate load, the equivalent damping coefficient was about 0.1 for the reinforced concrete joint and was about 0.3 for SRC. While for the specimen tested in this study the equivalent coefficient was about 0.192-0.279. This indicated that the energy-dissipation capacity of the tested joints was excellent and can meet the requirement of seismic design.
- The energy ratio was larger, which indicated that past ultimate load, the energy-dissipation capacity remained good. The energy ratio of SLJ-2, SLJ-3 was higher than that of SLJ-1. According to the previous results, the energy ratio of the reinforced concrete structure and steel structure under damage load was 10, and 40, respectively (Sivaselvan and Reinhorn 2000, Song and Pincheira 2000), which indicated that the specimen with viscous dampers had better energy-

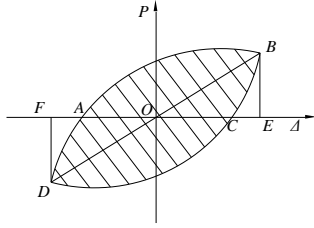


Fig. 14 Sketch of counting methods for equivalent damping coefficient

Table 6 Index of energy dissipation

Specimen No.	h_e		I_w
	Yield	Ultimate	Failure
SLJ-1	0.144	0.192	0.223
SLJ-2	0.197	0.271	0.392
SLJ-3	0.187	0.279	0.397

dissipation capacity than the reinforced concrete structure. The installation of dampers can greatly improve the global seismic behaviors and mechanic properties.

The energy-dissipation capacity is expressed by the equivalent damping coefficient, h_e , and the energy ratio, I_w (Gosain *et al.* 1977), the formula of equivalent damping coefficient as shown in the Eq. (3) below.

$$h_e = \frac{E_d}{2\pi}, \quad E_d = \frac{S_{(ABC+CDA)}}{S_{(\Delta OBE+\Delta ODF)}} \quad (3)$$

Where, h_e refers to the equivalent damping coefficient; E_d refers to the energy dissipation coefficient; $S_{(ABC+CDA)}$ refers to combined of shaded part area be encircled by hysteresis loop; $S_{(\Delta OBE+\Delta ODF)}$ refers to combined of area of the triangle in Fig. 14.

4.5 The analysis of degradation of stiffness

The degradation of stiffness of the structure under different loading cycles with the same displacement can be expressed by secant stiffness, K_i , which can be calculated by the Eq. (3) below. K_i is the ratio of the sum of the absolute value to the corresponding sum of absolute deformation.

$$K_i = \frac{|+P_i| + |-P_i|}{|+\Delta_i| + |-\Delta_i|} \quad (3)$$

Where, $+P_i(-P_i)$ refers to the peak load under cycle i ; and $+\Delta_i(-\Delta_i)$, the corresponding displacement.

Fig. 15 shows the calculation of K_i under different loading displacement.

Only the stiffness during the period ranging from the elasto-plastic to the damage stage was selected as the research object, because there was no obvious stiffness degradation during the elastic period. Based on the results indicated in Fig. 10, we can conclude that:

- With the increase of the displacement, the stiffness decreased, reflecting the stiffness degradation under cycle-

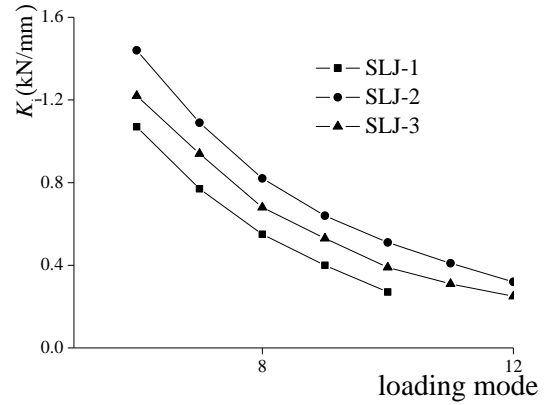


Fig. 15 Curves of stiffness degradation

reversed load. The reason accounting for this phenomenon was that with the increase of the load, the accumulative damage increased, resulting in the spalling of concrete and the yielding of reinforcement.

- The degradation curves were nearly parallel to each other, indicating that the degradation law of each specimen was almost the same. The degradation appeared to be quicker after yielding, but ending in stable condition.

- Although the degradation law of specimen SLJ-2, SLJ-3 was similar, when the degradation happened, the stiffness of SLJ-3 was lower than that of SLJ-2. This indicated that no direct relationship between the stiffness degradation and the design load of the viscous damper.

5. Conclusions

In this paper, a new type of joint which is combination of concrete archaized building with viscous damper was put forward. Two specimens with viscous damper were defined as the controlled component and one specimen without viscous damper was specified as the non-controlled component. The overall failure process and failure mode were obtained. The mechanical behaviors and seismic performances of the joints were analyzed. The results indicate that the joint with viscous damper has good seismic behaviors and energy dissipation behavior. The following conclusions can be drawn:

- The failure modes of all the specimens were beam-hinged mechanism. The layout of the viscous dampers has a large influence on the damage process. For uncontrolled component with no damper, the specimen became deformable mechanism of beam-hinges, resulting in the termination of experiment for being not suitable for continuing load carrying; While for controlled component with viscous damper, the specimen remained stable since the damper can serve as brace when the beam-hinged mechanism emerged.

- The viscous damper can improve the bearing capacity and energy-dissipation capacity of the specimen greatly, resulting in the increase of ductility to some extent.

- When the failure of specimen with viscous damper occurred, it can be found that its energy-dissipation capacity was better than that of the ordinary reinforced concrete frame with the ductility $\mu=3.02-3.28$, equivalent damping

coefficient $h_c=0.392-0.397$ as well as energy coefficient $I_w=16.4-19.8$.

- After achieving the yield load, the descending ratio increased gradually, then the stiffness become stable. For the controlled component, there was no direct relationship between the stiffness degradation and the design load of the viscous damper.

- Due to the uncertainties involved in the construction of the joints and installation of the viscous damper, particularly the gaps within the linking region of viscous damper and joint, further work is required to eradicate the adverse effect.

6. Suggestions

- Although some initial results of viscous damper on concrete archaized building with lintel-column joint has been achieved, there are still many problems should to be solved. Such as how to design and choose the type of viscous damper and its parameters in practical project, how to ensure the effectiveness, stability and security of viscous damper.

- It is suggested that numerical simulation and analysis of the viscous damper on Chinese traditional style structure with dual-lintel-column joint of steel and composite structures should be analyzed before the type of viscous damper and its parameters are confirmed.

Acknowledgments

The authors would like to thank the National Natural Science Foundation of China (Grant No. 51678478, 51208411), Shaanxi Science and Technology Research and Development Projects (Grant No. 2013KW23-01) and Innovative Research Team Foundation of Xi'an University of Architecture and Technology for their generous supports of this study.

References

- Abdi, H., Hejazi, F., Saifulnaz, R., Karim, I.A. and Jaafar, M.S. (2015), "Response modification factor for steel structure equipped with viscous damper device", *J. Steel Struct.*, **15**(3), 605-622.
- Elnashai, A.S., Broderick, B.M. and Dowling, P.J. (1995), "Earthquake-resistant composite steel/concrete structures", *Struct. Eng.*, **73**, 121-121.
- GB 50011 (2010), *Code for Seismic Design of Buildings*, Ministry of Housing and Urban-Rural Development, Beijing, China
- GB/T 17742 (2008), *The Chinese Seismic Intensity Scale*, Ministry of Housing and Urban-Rural Development, Beijing, China.
- Gosain, N.K., Jirsa, J.O. and Brown, R.H. (1977), "Shear requirements for load reversals on RC members", *J. Struct. Div.*, **103**(7), 1461-1476.
- Han, L.H. (2007), *CFST Structure: Theory and Practice*, Science Press, Beijing, China.
- Housner, G.W., Bergman, L., Caughey, T.K., Chassiakos, A.G., Claus, R.O., Masri, S.F. and Yao, J.T. (1997), "Structural control: past, present, and future", *J. Eng. Mech.*, **123**(9), 897-971.
- JGT 209 (2012), *Dampers for Vibration Energy Dissipation of Buildings*, Ministry of Housing and Urban-Rural Development, Beijing, China.
- Li, P. (2014), "Experimental study on seismic behavior of RC column-beam joint built in traditional style", M.Sc. Dissertation, Xi'an University of Architecture & Technology, Xi'an, China.
- Parmar, A., Patel, V., Kotak, B. and Patel, M. (2014), "Seismic response control of asymmetric building using VISCOUS DAMPER", *J. Civil Eng. Technol.*, **5**(12), 267-276.
- Sivaselvan, M.V. and Reinhorn, A.M. (2000), "Hysteretic models for deteriorating inelastic structures", *J. Eng. Mech.*, **126**(6), 633-640.
- Song, J.K. and Pincheira, J. (2000), "Spectral displacement demands of stiffness-and strength-degrading systems", *Earthq. Spectr.*, **16**(4), 817-851.
- Song, Z.B. (2001), "The application of viscous damping energy consumption technology in structural seismic strengthening", M.Sc. Dissertation, China Academy of Building Research, Beijing, China.
- Tian, Y.F. (2012), *Building Construction of Chinese Imitated Ancient Building*, Chemical Industry Press, Beijing, China.
- Wang, C.X., Xu, K. and Tian, L.Q. (2011), "Structure design of mingtang for protection of the ruins of ancient buildings built in the Sui and Tang Dynasty in Luoyang City", *Steel Constr.*, **26**(8), 26-31.
- Xie, L. (2006), "Study on application of imitations of traditional Chinese architecture in landscape architecture", M.Sc. Dissertation, Zhejiang A&F University, Hangzhou, China.
- Xie, Q.F., Li, P., Ge, H.P., Sui, Y. and Wu, K. (2015), "Experimental study on seismic behavior of RC column-beam joint built in traditional style", *World Earthq. Eng.*, **31**(4), 150-158.
- Xue, J.Y., Wu, Z.J., Sui, Y. and Liu, Z.Q. (2015), "Experimental study on seismic performance of steel double-beams column exterior joints in antique style building", *J. Build. Struct.*, **36**(3), 80-89.
- Xue, J.Y., Wu, Z.J., Sui, Y., Ge, H.P. and Wu, K. (2016), "Experimental study and numerical analysis on aseismic performance of steel double-beam-column interior-joints in traditional style building", *Eng. Mech.*, **33**(5), 97-105.
- Zheng, Z.C., Moritaka, H. and Shimoda, K. (2006), "The seismic retrofit of the Kagoshima airport terminal building-the 3D inelastic analysis of the structure with viscous damper walls", *Build. Struct.*, **30**(6), 19-26.
- Zhu, D.S., Li, X. and Chang, S. (2014), "Seismic response control of viscous damper on concrete-filled steel tubular frame Piers", *J. Chongqing Jiaotong Univ.*, **33**(4), 1-6.

CC